Volume 12
Number 20
28 May 2021
Pages 6759–7198

Chemical Science

rsc.li/chemical-science

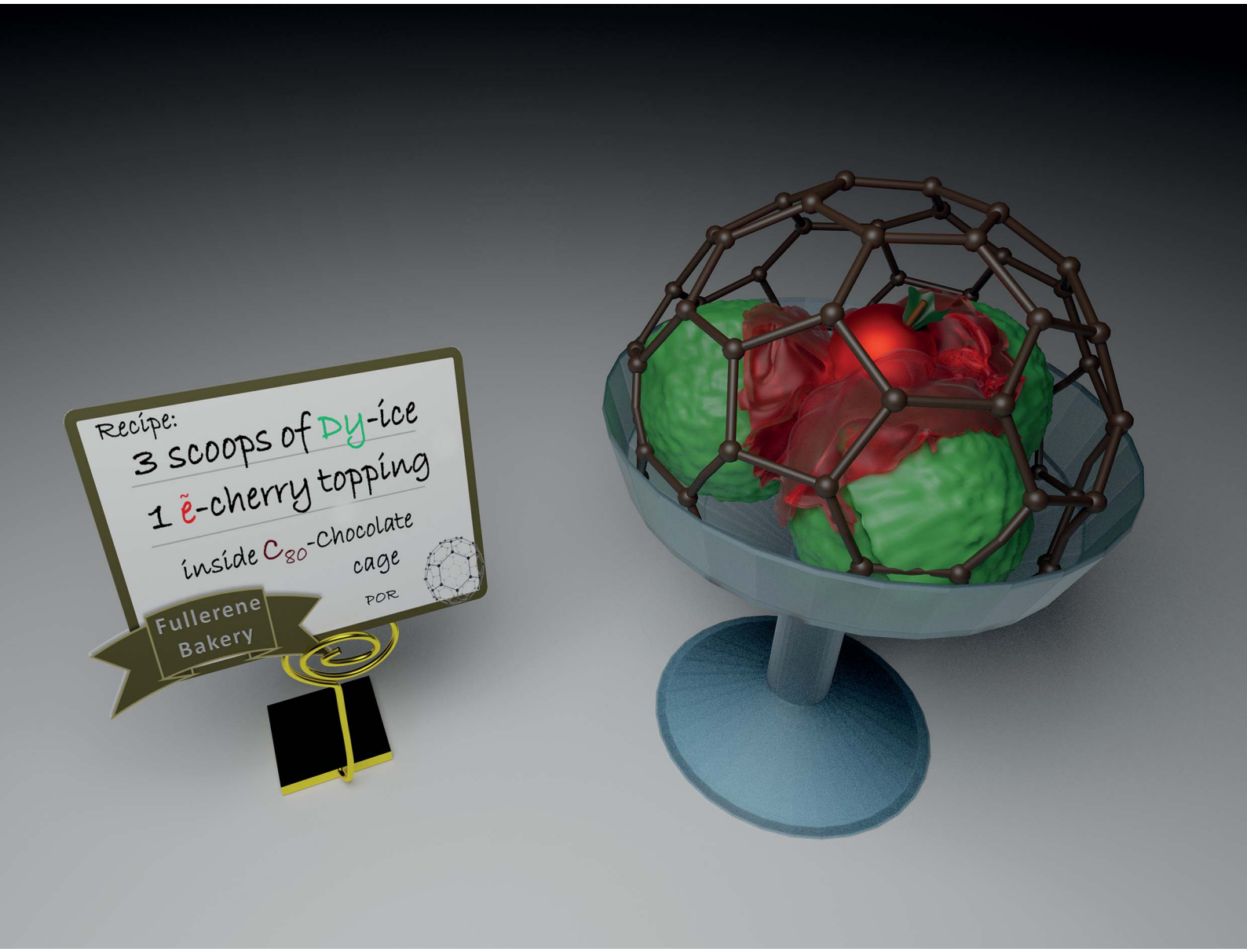

ISSN 2041-6539

ROYAL SOCIETY OF CHEMISTRY

EDGE ARTICLE

Muqing Chen, Qianyan Zhang, Alexey A. Popov, Shangfeng Yang *et al.*

Stabilizing a three-center single-electron metal–metal bond in a fullerene cage

Chemical Science

ROYAL SOCIETY OF CHEMISTRY

EDGE ARTICLE

View Article Online
View Journal | View Issue

Cite this: *Chem. Sci.*, 2021, **12**, 6890

All publication charges for this article have been paid for by the Royal Society of Chemistry

Received 18th February 2021
Accepted 31st March 2021

DOI: 10.1039/d1sc00965f

rsc.li/chemical-science

Stabilizing a three-center single-electron metal–metal bond in a fullerene cage†

Fei Jin,‡[a] Jinpeng Xin,‡[a] Runnan Guan,[a] Xiao-Ming Xie,[b] Muqing Chen, *[a] Qianyan Zhang,*[b] Alexey A. Popov, *[c] Su-Yuan Xie[b] and Shangfeng Yang *[a]

Trimetallic carbide clusterfullerenes (TCCFs) encapsulating a quinary M_3C_2 cluster represent a special family of endohedral fullerenes with an open-shell electronic configuration. Herein, a novel TCCF based on a medium-sized rare earth metal, dysprosium (Dy), is synthesized for the first time. The molecular structure of $Dy_3C_2@I_h(7)$-C_{80} determined by single crystal X-ray diffraction shows that the encapsulated Dy_3C_2 cluster adopts a bat ray configuration, in which the acetylide unit C_2 is elevated above the Dy_3 plane by ~1.66 Å, while Dy–Dy distances are ~3.4 Å. DFT computational analysis of the electronic structure reveals that the endohedral cluster has an unusual formal charge distribution of $(Dy_3)^{8+}(C_2)^{2-}@C_{80}{}^{6-}$ and features an unprecedented three-center single-electron Dy–Dy–Dy bond, which has never been reported for lanthanide compounds. Moreover, this electronic structure is different from that of the analogous $Sc_3C_2@I_h(7)$-C_{80} with a $(Sc_3)^{9+}(C_2)^{3-}@C_{80}{}^{6-}$ charge distribution and no metal–metal bonding.

Introduction

Endohedral clusterfullerenes featuring encapsulation of an unstable metallic cluster within a fullerene cage have been attracting considerable interest over the past two decades due to the versatility of the types of encapsulated cluster and its charge transfer to the outer fullerene cage.[1–8] Soon after the discovery of $Sc_3N@C_{80}$ as the first endohedral clusterfullerene encapsulating a trimetallic nitride cluster in 1999,[9] the first metal carbide clusterfullerene (CCF), $Sc_2C_2@C_{84}$, was identified by Shinohara and coworkers in 2001.[10] The identification that a C_2 moiety can be encapsulated in the form of metal carbide revealed a competition between CCFs $M_2C_2@C_{2n-2}$ and genuine dimetallofullerenes (di-EMFs) $M_2@C_{2n}$ in the hot carbon vapor during the fullerene formation. Importantly, CCFs and di-EMFs have different electronic structures and metal valence states. For Sc, Y, and heavy lanthanides, di-EMFs feature a $(M_2)^{4+}@C_{2n}{}^{4-}$ distribution with M–M bonding and formally divalent metal M^{2+},[11–14] while the charge distribution in dimetallic CCFs is $(M_2)^{6+}(C_2)^{2-}@C_{2n}{}^{4-}$ with the more traditional M^{3+} state of rare-earth metals.[8,15,16] Thus, by accumulating a certain negative charge, the C_2 group has a paramount influence on the valence state of endohedral metal atoms.

The C_2 group in CCFs has a variable formal charge state adapting to the metal cluster composition, from $(C_2)^{2-}$ in $M_2C_2@C_{2n}$ to $(C_2)^{6-}$ in $Sc_4C_2@C_{80}$.[17,18] In $Sc_3C_2@C_{80}$, the first trimetallic CCF (TCCF) and the only TCCF characterized by single-crystal X-ray diffraction (SC-XRD),[19] the acetylide unit has a formal $(C_2)^{3-}$ charge state.[20] A similar charge distribution is also proposed for $Lu_3C_2@C_{88}$.[21] In mixed-metal $M_2TiC_2@C_{80}$ TCCFs (M = Sc, Lu, Dy), the acetylide unit adopts a $(C_2)^{4-}$ state to balance the tetravalent Ti^{4+}.[22,23] In these five TCCFs, rare-earth metals are present in their 3+ oxidation state and thus do not form metal–metal bonding interactions. Interestingly, three-center M–M bonding was predicted in $Y_3@C_{80}$ and $Er_3@C_{74}$ trimetallofullerenes (tri-EMFs) based on computational analysis, but structural characterization of such tri-EMFs is still lacking.[24,25]

In this work, we aim at filling the gap in the knowledge about rare-earth TCCFs and synthesized a novel TCCF based on a medium-sized rare-earth metal, dysprosium (Dy) – $Dy_3C_2@C_{80}$. Astonishingly, SC-XRD and computational analysis of $Dy_3C_2@C_{80}$ revealed that, dramatically different from the analogous $Sc_3C_2@C_{80}$ based on the small-sized metal Sc, $Dy_3C_2@C_{80}$ exhibits an unusual $(Dy_3)^{8+}(C_2)^{2-}@C_{80}{}^{6-}$ formal charge distribution and features a unique three-center single-electron Dy–Dy–Dy bond, which has never been reported in molecular lanthanide chemistry.[26–28]

[a]*Hefei National Laboratory for Physical Sciences at Microscale, CAS Key Laboratory of Materials for Energy Conversion, Department of Materials Science and Engineering, Synergetic Innovation Center of Quantum Information & Quantum Physics, University of Science and Technology of China, Hefei 230026, China. E-mail: sfyang@ustc.edu.cn*

[b]*State Key Lab for Physical Chemistry of Solid Surfaces, Collaborative Innovation Center of Chemistry for Energy Mate-rials, Department of Chemistry, College of Chemistry and Chemical Engineering, Xiamen University, Xiamen 361005, China*

[c]*Leibniz Institute for Solid State and Materials Research (IFW Dresden), Helmholtzstrasse 20, Dresden, 01069, Germany*

† Electronic supplementary information (ESI) available. CCDC 2057452. For ESI and crystallographic data in CIF or other electronic format see DOI: 10.1039/d1sc00965f

‡ These authors contributed equally to this work.

Results and discussion

Synthesis, isolation and molecular structure of $Dy_3C_2@I_h(7)$-C_{80}

$Dy_3C_2@C_{80}$ was synthesized by a modified Krätschmer–Huffman DC arc discharge method using a mixture of Dy_2O_3 and graphite (molar ratio of Dy : Ti : C = 1 : 1 : 15) as the raw material under 200 mbar He and 10 mbar N_2 gas.[29–32] Isolation of $Dy_3C_2@C_{80}$ was fulfilled by three-step HPLC (see ESI S1† for details). The purity of the isolated $Dy_3C_2@C_{80}$ was confirmed by laser desorption time-of-flight (LD-TOF) mass spectroscopic (MS) and HPLC analyses (Fig. 1a and b). The LD-TOF MS spectrum shows a dominant mass peak at $m/z = 1471.5$ with the isotopic distribution resembling the calculated one for Dy_3C_{82}. The HPLC profile with a single peak at a retention time of 53.5 min confirms the high purity of the isolated Dy_3C_{82}. Based on the integrated area of the corresponding HPLC peaks, the yield of Dy_3C_{82} relative to $Dy_3N@I_h(7)$-C_{80} is estimated to be 1 : 320 (see ESI Table S1†).

The molecular structure of Dy_3C_{82} was established by SC-XRD using co-crystallization with a recently developed decapyrrylcorannulene (DPC) host.[33] Mixing a CS_2 solution of fullerene with a toluene solution of DPC afforded cocrystal $Dy_3C_2@I_h(7)$-$C_{80}\cdot 2(DPC)\cdot 3(C_7H_8)$, and its SC-XRD analysis confirmed unambiguously that the isolated Dy_3C_{82} is $Dy_3C_2@I_h(7)$-C_{80} TCCF. The cocrystal falls into the monoclinic $P2_1/c$ space group, its asymmetric unit cell is composed of four complete $Dy_3C_2@I_h$-C_{80} fullerene molecules and four pairs of 2DPC. Fig. 1c illustrates the relative orientations of the $Dy_3C_2@I_h(7)$-C_{80} and the DPC molecules in the cocrystal, in which only one orientation of the fullerene cage together with the major site of the Dy_3C_2 cluster is shown for clarity. The nearest DPC-cage distances are 3.322(11) and 3.341(12) Å, respectively, which are comparable to those of the cocrystals of DPC with other endohedral fullerenes.[33] It is noteworthy that so far only two TCCFs with a homometallic M_3C_2 cluster have been

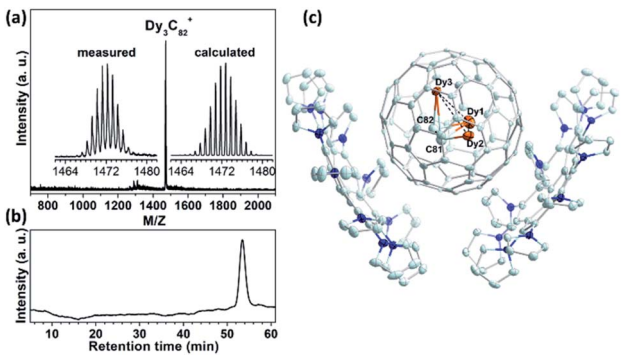

Fig. 1 Confirmation of the purity and determination of the molecular structure of $Dy_3C_2@I_h$-C_{80}. (a) LD-TOF mass spectrum of purified $Dy_3C_2@I_h$-C_{80}; the insets show the measured and calculated isotopic distributions of Dy_3C_{82}. (b) HPLC profile of fraction A-3-3 (4.6 × 250 mm Buckyprep column; toluene as an eluent; flow rate 1.0 ml min^{-1}; injection volume 1 ml; 25 °C). (c) The thermal ellipsoid drawing of $Dy_3C_2@I_h(7)$-$C_{80}\cdot$2DPC. Only the major Dy_3C_2 site is shown. Solvent molecules and H atoms are omitted for clarity.

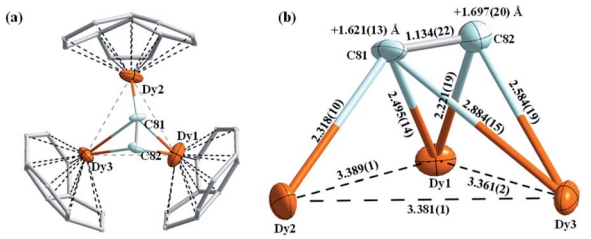

Fig. 2 Configuration of the Dy_3C_2 cluster within $Dy_3C_2@I_h(7)$-C_{80}. (a) Position of the Dy_3C_2 cluster within $Dy_3C_2@I_h(7)$-C_{80} (major Dy sites) with the closest fullerene fragments. (b) The geometric structure of the Dy_3C_2 cluster with bond lengths determined by single-crystal X-ray diffraction. The numbers above the carbon atoms indicate the vertical displacements of carbon atoms above the Dy_3 planes. Distances are in Å. C and Dy atoms are shown in cyan and orange, respectively.

reported, $Sc_3C_2@I_h(7)$-C_{80} (ref. 19 and 34–38) and $Lu_3C_2@D_2(35)$-C_{88},[21] both with rare-earth metals of relatively small ionic radius (R^{3+} is 0.75 Å for Sc and 0.86 Å for Lu[39]), and only $Sc_3C_2@I_h(7)$-C_{80} has been structurally determined by SC-XRD.[19] Therefore, $Dy_3C_2@I_h(7)$-C_{80} represents the first TCCF based on a medium-sized rare-earth metal ($R(Dy^{3+}) = 0.91$ Å) with the molecular structure determined unambiguously by SC-XRD.

While the $I_h(7)$-C_{80} cage is fully ordered in the crystal, Dy atoms are disordered over 14 positions, whose site occupancies range from 0.051(2) to 0.501(2) (see ESI Fig. S2b†). The further structural analysis is based on the major Dy1–Dy3 sites with the largest occupancies of 0.482(2), 0.501(2) and 0.429(3), respectively. Dy atoms are located near the junctions of one pentagon and two hexagons as shown in Fig. 2a, with the shortest Dy–C(cage) distances of 2.202(16), 2.253(12), and 2.254(9) Å, suggesting a strong metal–cage interaction. The Dy···Dy distances are 3.381(1), 3.361(2), and 3.389(1) Å, respectively, which are all shorter than Sc···Sc distances in $Sc_3C_2@I_h(7)$-C_{80} (3.407(3), 3.712(3), and 3.989(3) Å)[19] or Dy···Dy distances in $Dy_3N@I_h(7)$-C_{80} (3.476(3), 3.541(3), and 3.564(3) Å).[40]

In view of a considerable disorder of heavy Dy atoms, positions of endohedral carbons are not very well defined. The best refinement results were obtained for a bat ray configuration of the Dy_3C_2 cluster shown in Fig. 2. The center of the C_2 unit is elevated above the Dy1–Dy2–Dy3 plane by ~1.66 Å. The bat ray configuration was also found in the SC-XRD study of $Sc_3C_2@I_h(7)$-C_{80}, but the elevation of the C_2 unit above the Sc_3 plane is considerably smaller (0.44 Å).[19] Besides, the C–C distance within the Dy_3C_2 cluster is determined to be 1.134(22) Å, which is smaller than that within Sc_3C_2 (1.29(3) Å (ref. 19)). Overall, these results reveal the strong influence of the metal size on the geometry of the encapsulated M_3C_2 cluster within the TCCF. The rare earth metals with larger size push the C_2 unit further above the M_3 plane and at the same time afford shorter M···M distances.

DFT computational studies of $M_3C_2@I_h(7)$-C_{80} (M = Dy, Sc)

The different shapes of the Dy_3C_2 and Sc_3C_2 clusters motivated us to conduct a DFT computational study (Priroda and Orca codes[41,42]) of the molecular and electronic structure of

$M_3C_2@C_{80}$ (M = Dy, Sc) molecules. In $Sc_3C_2@C_{80}$, earlier computations and SC-XRD studies revealed two quasi-isoenergetic structures of the Sc_3C_2 unit.[19,20] In the lower-energy bat ray configuration, the C_2 unit is almost parallel to the Sc_3 plane and is elevated above it (Fig. 3a). The trifoliate structure has a trigonal bipyramidal shape with the Sc_3 triangle in the base and two C atoms in the apexes. Using these structures as starting configurations for optimization of $Dy_3C_2@C_{80}$ showed that Dy_3C_2 also has a minimum for a trifoliate configuration albeit with high relative energy, but the bat ray configuration changed considerably during optimization by elevating the C_2 unit by 1.620 Å above the Dy_3 plane and giving a structure quite similar to that found by SC-XRD. Analogous results were obtained in computations of $Y_3C_2@C_{80}$ (see the ESI†). Thus, the larger ionic radii of Dy^{3+} and Y^{3+} do not afford enough place for the C_2 unit when it is too close to the M_3 plane. Importantly, this bat ray structure of the Dy_3C_2 cluster is 89 kJ mol^{-1} more stable than the trifoliate configuration. Different positions of the C_2 group also result in substantial differences in the DFT-optimized Dy⋯Dy distances. For the bat ray structure, the predicted distances of 3.440, 3.382, and 3.408 Å agree well with the SC-XRD results, while the trifoliate configuration has longer Dy⋯Dy distances of 3.637, 3.651, and 3.939 Å. The transition state connecting these two cluster configurations is found at a relative energy of 140 kJ mol^{-1}. The bat ray structure with an elevated C_2 unit similar to the Dy_3C_2 cluster is also found to be

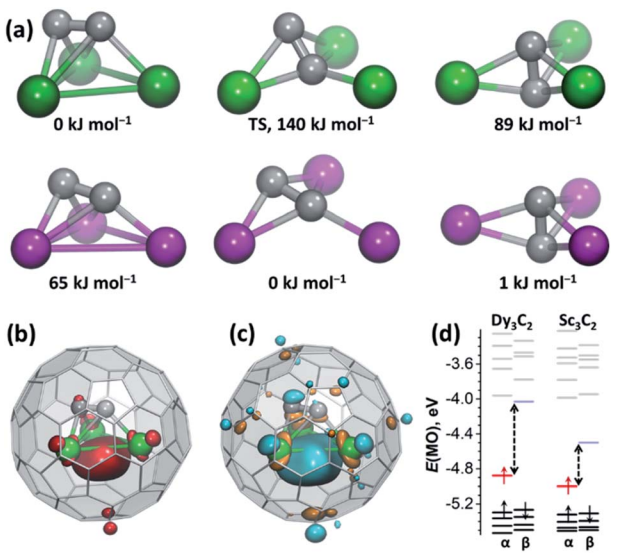

Fig. 3 DFT computational study on the electronic structure of $M_3C_2@C_{80}$ (M = Dy, Sc). (a) DFT-optimized configurations of the Dy_3C_2 (top) and Sc_3C_2 (bottom) clusters in $M_3C_2@C_{80}$ and their relative energies. Dy is depicted in green, Sc is shown in magenta, and "TS" means transition state. (b) DFT-computed valence spin density distribution in $Dy_3C_2@C_{80}$. (c) Singly occupied MO (SOMO) in $Dy_3C_2@C_{80}$. (d) Kohn–Sham MO energy levels in the lowest energy configurations of $Dy_3C_2@C_{80}$ and $Sc_3C_2@C_{80}$ (red and pale blue lines denote the occupied and unoccupied components of the singly occupied MO, and dashed arrows highlight the gap between the SOMO components). Computations are performed with the PBE functional, def2-TZVPP basis set for C and Sc, and 4f-in-core ECP55MWB-II basis set of Dolg and coworkers for Dy.[43–46]

an energy minimum for $Sc_3C_2@C_{80}$, but this configuration is 65 kJ mol^{-1} less stable than the trifoliate and flattened bat-ray configurations. Thus, in agreement with the experimental results, our calculations confirm that the lowest energy configuration of the Dy_3C_2 cluster has relatively short Dy⋯Dy distances and a significantly elevated position of the C_2 unit, which is different from the optimal geometry of the Sc_3C_2 cluster.

Confinement of the Dy_3C_2 cluster within the I_h-C_{80} cage not only changes the molecular structure in comparison to the Sc congener, but also results in a completely new bonding situation. Previous studies showed that the electronic configuration of $Sc_3C_2@C_{80}$ is best described as $(Sc_3)^{9+}(C_2)^{3-}@C_{80}^{6-}$ with the spin density mainly localized on the C_2^{3-} unit and Sc atoms featuring their typical Sc^{3+} oxidation state.[20] Surprisingly, in the Dy analog the charge distribution changes to $(Dy_3)^{8+}(C_2)^{2-}@C_{80}^{6-}$ (see ESI S5† for the analysis of the canonical and Pipek–Mezey localized orbitals of the cluster). Acetylide unit C_2 in $Dy_3C_2@C_{80}$ has negligible spin population, while the main part of spin density is shared between three Dy ions (Fig. 3b). This spin distribution reflects the shape of the SOMO, which has Dy–Dy–Dy bonding character and corresponds to the three-center single-electron bonding of all three Dy atoms (Fig. 3c) with main contributions from the 6s, 6p, and 5d atomic orbitals of Dy. The presence of the M–M bonding in medium-size rare-earth $M_3C_2@C_{80}$ TCCFs is further corroborated by topological analysis of the electron density as described in the ESI.† Dimetallofullerenes were already shown to stabilize unique single-electron lanthanide–lanthanide bonds.[47–50] $Dy_3C_2@C_{80}$ described in this work is the first example of the new lanthanide bonding motif, *i.e.*, three-center single-electron Dy–Dy–Dy bond. Three-center metal–metal bonding was earlier predicted in trimetallofullerene $Y_3@C_{80}$, but in this molecule the Y–Y–Y bonding MO is occupied by two electrons.[22,23] Interestingly, $Dy_3C_2@C_{80}$ with a trifoliate cluster configuration has a more traditional $(Dy_3)^{9+}(C_2)^{3-}@C_{80}^{6-}$ electron distribution without metal–metal bonding (see the ESI† for further analysis). Thus, variation of the C_2 unit position within the M_3C_2 cluster has a strong influence on the valence state of metal atoms.

To clarify whether the shape of the Dy_3C_2 cluster in $Dy_3C_2@C_{80}$ results from the templating effect of the fullerene cage or has a universal character for rare-earth TCCFs, we performed optimization of the molecule with a larger fullerene cage, $Y_3C_2@C_{88}$ (Y^{3+} has a comparable ionic radius (0.90 Å) to Dy^{3+}). Three different shapes of the cluster were used in the starting configurations: trifoliate, planar bat ray, and bat ray with an elevated C_2 unit like in $Dy_3C_2@C_{80}$. In all cases, optimization converged to the structure with a flattened bat ray configuration, and re-optimization of the latter with Dy instead of Y also left the shape intact (see ESI Fig. S4†). This result agrees with the earlier study of $Lu_3C_2@C_{88}$, which predicted a planar shape of the Lu_3C_2 cluster, with the C_2 unit lying in the triangle plane of three metals.[21] Finally, an earlier computational study of $Y_3C_2@C_{96}$ also favoured the flattened shape of the cluster.[24] Based on these results, we conclude that the unique structure of the Dy_3C_2 cluster supporting the Dy–Dy–Dy bonding in $Dy_3C_2@C_{80}$ is a result of the favourable

matching between the fullerene cage size and metal size. When the metal is smaller like Sc or the fullerene cage has a larger inner space (say, C_{88} or C_{96}), the M_3C_2 cluster tends to adopt a flattened bat ray shape, which does not lead to direct metal–metal bonding.

Electronic properties of $Dy_3C_2@I_h(7)$-C_{80}

We next characterized the electronic properties of $Dy_3C_2@I_h(7)$-C_{80} by UV-vis-NIR spectroscopy and electrochemistry (Fig. 4). The electronic absorption spectrum of yellow $Dy_3C_2@I_h(7)$-C_{80} solution in toluene looks featureless without discernible absorption peaks and is similar to the spectrum of $Sc_3C_2@I_h(7)$-C_{80}. Both compounds have their absorption onset at around 850–900 nm (Fig. 4a). Electrochemical characterization by cyclic voltammetry (CV) and differential pulse voltammetry (DPV) gives more distinct characteristics of the compound (Fig. 4b). $Dy_3C_2@I_h(7)$-C_{80} exhibits one reversible oxidation step at +0.19 V, one reversible reduction step at $E_{1/2} = -0.99$ V, and one irreversible reduction with a peak potential of −1.65 V. The electrochemical gap ΔE_{EC} of $Dy_3C_2@I_h(7)$-C_{80} is thus 1.18 V. It is remarkable that the ΔE_{EC} gap of $Sc_3C_2@I_h(7)$-C_{80} is only 0.47 V, as its first oxidation and reduction potentials are found at −0.03 V and −0.50 V, respectively (see ESI Fig. S10 and Table S6†).[34] Both TCCFs have their SOMO localized on the M_3C_2 cluster, but their different electronic configurations result in a considerable difference of the frontier MO energies (Fig. 3d).

The Dy–Dy–Dy-bonding nature of the SOMO in $(Dy_3)^{8+}$ indicates that reduction and oxidation should substantially change the Dy–Dy bonding situation in $Dy_3C_2@I_h(7)$-C_{80}. Indeed, DFT calculations show that Dy–Dy bond lengths in the anion shorten to 3.363/3.366/3.320 Å as a result of the stronger Dy–Dy bonding provided by the population of the Dy_3-bonding MO by the second electron in the $(Dy_3)^{7+}$ fragment. In the $Dy_3C_2@C_{80}^+$ cation, the Dy–Dy distances increase to 3.668/3.473/3.542 Å as the metal–metal bonding is diminished when the Dy_3-bonding MO is completely depopulated in $(Dy_3)^{9+}$. The electrochemical gap of 1.10 V estimated by DFT with the polarized continuum model of the solvent agrees well with the experimental value, confirming the reliable interpretation of the redox process by theory.

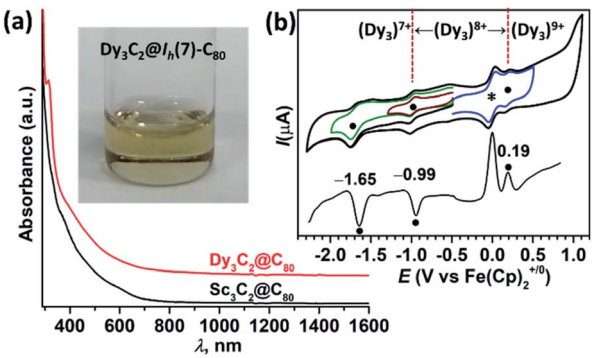

Fig. 4 Electronic properties of $Dy_3C_2@I_h(7)$-C_{80}. (a) UV-vis-NIR absorption spectra of $Dy_3C_2@I_h(7)$-C_{80} and $Sc_3C_2@I_h(7)$-C_{80} dissolved in toluene. Inset: the photograph of $Dy_3C_2@I_h(7)$-C_{80} solution in toluene. (b) Cyclic voltammogram (top) and differential pulse voltammogram (bottom) of $Dy_3C_2@I_h(7)$-C_{80} measured in *o*-DCB solution with $TBAPF_6$ as the supporting electrolyte (scan rate: 100 mV s^{-1}); ferrocene $Fe(Cp)_2$ was added as the internal standard. Each redox step of $Dy_3C_2@C_{80}$ is marked with a solid dot; the asterisk denotes the oxidation peak of ferrocene. Variation of the formal charge of the Dy_3 fragment in different potential ranges is indicated.

Conclusions

In summary, for the first time we synthesized and isolated a novel TCCF based on a medium-sized rare-earth metal, dysprosium (Dy) – $Dy_3C_2@I_h(7)$-C_{80}. Its molecular structure elucidated by SC-XRD reveals Dy_3C_2 with a bat ray configuration similar to $Sc_3C_2@C_{80}$. But the larger size of Dy pushes the acetylide unit above the Dy_3 plane and at the same time results in shorter Dy–Dy distances than Sc–Sc distances in $Sc_3C_2@C_{80}$. The electronic configuration of $Dy_3C_2@C_{80}$ is described as $(Dy_3)^{8+}(C_2)^{2-}@C_{80}{}^{6-}$ and features a unique three-center single-electron Dy–Dy–Dy bond, which represents the first example of such bonding motif in molecular lanthanide chemistry. Furthermore, the population of the Dy–Dy–Dy-bonding SOMO can be changed electrochemically, providing access to ionic species with either strengthened or weakened Dy–Dy bonds. Our finding on the unprecedented three-center single-electron metal–metal bond offers new insight into the bonding theory of lanthanide coordination compounds.

Author contributions

S. F. Y. conceived and designed this research. F. J. and J. P. X. synthesized, isolated the samples and conducted characterizations. R. N. G. helped with sample separation and characterizations. M. Q. C. helped with X-ray crystallographic measurements. A. A. P. did the DFT calculations. X. M. X., Q. Y. Z. and S. Y. X. afforded decapyrrylcorannulene. F. J., J. P. X., A. A. P. and S. F. Y. co-wrote the paper, and all the authors commented on it.

Conflicts of interest

There are no conflicts to declare.

Acknowledgements

This work was partially supported by the National Key Research and Development Program of China (2017YFA0402800), National Natural Science Foundation of China (51925206, U1932214, 21721001 and 91961113), and Deutsche Forschungsgemeinschaft (PO 1602/5 and PO 1602/7). We thank the staff of the BL17B beamline of the National Facility for Protein Science Shanghai (NFPS) at the Shanghai Synchrotron Radiation Facility for assistance during data collection and Ulrike Nitzsche for assistance with computational resources at IFW Dresden.

Notes and references

1 S. Yang, F. Liu, C. Chen, M. Jiao and T. Wei, *Chem. Commun.*, 2011, **47**, 11822–11839.
2 A. A. Popov, S. Yang and L. Dunsch, *Chem. Rev.*, 2013, **113**, 5989–6113.
3 X. Lu, L. Feng, T. Akasaka and S. Nagase, *Chem. Soc. Rev.*, 2012, **41**, 7723–7760.
4 S. Yang, T. Wei and F. Jin, *Chem. Soc. Rev.*, 2017, **46**, 5005–5058.
5 R. Guan, M. Chen, F. Jin and S. Yang, *Angew. Chem., Int. Ed.*, 2020, **59**, 1048–1073.
6 P. Yu, W. Shen, L. Bao, C. Pan, Z. Slanina and X. Lu, *Chem. Sci.*, 2019, **10**, 10925–10930.
7 D. Hao, L. Yang, B. Li, Q. Hou, L. Li and P. Jin, *J. Phys. Chem. A*, 2020, **124**, 2694–2699.
8 W. Shen, S. Hu and X. Lu, *Chem.–Eur. J.*, 2020, **26**, 5748–5757.
9 S. Stevenson, G. Rice, T. Glass, K. Harich, F. Cromer, M. R. Jordan, J. Craft, E. Hadju, R. Bible, M. M. Olmstead, K. Maitra, A. J. Fisher, A. L. Balch and H. C. Dorn, *Nature*, 1999, **401**, 55–57.
10 C. R. Wang, T. Kai, T. Tomiyama, T. Yoshida, Y. Kobayashi, E. Nishibori, M. Takata, M. Sakata and H. Shinohara, *Angew. Chem., Int. Ed.*, 2001, **40**, 397–399.
11 A. A. Popov, S. M. Avdoshenko, A. M. Pendás and L. Dunsch, *Chem. Commun.*, 2012, **48**, 8031–8050.
12 W. Shen, L. Bao, Y. Wu, C. Pan, S. Zhao, H. Fang, Y. Xie, P. Jin, P. Peng, F.-F. Li and X. Lu, *J. Am. Chem. Soc.*, 2017, **139**, 9979–9984.
13 C. Pan, W. Shen, L. Yang, L. Bao, Z. Wei, P. Jin, H. Fang, Y.-P. Xie, T. Akasaka and X. Lu, *Chem. Sci.*, 2019, **10**, 4707–4713.
14 X. Lu, S. Hu, W. Shen, G. Duan, L. Yang, P. Jin, Y. Xie and T. Akasaka, *Chem.–Eur. J.*, 2019, **25**, 11538–11544.
15 P. Jin, C. Tang and Z. Chen, *Coord. Chem. Rev.*, 2014, **89**, 270–271.
16 X. Lu, T. Akasaka and S. Nagase, *Acc. Chem. Res.*, 2013, **46**, 1627–1635.
17 K. Tan, X. Lu and C. R. Wang, *J. Phys. Chem. B*, 2006, **110**, 11098–11102.
18 T.-S. Wang, N. Chen, J.-F. Xiang, B. Li, J.-Y. Wu, W. Xu, L. Jiang, K. Tan, C.-Y. Shu, X. Lu and C.-R. Wang, *J. Am. Chem. Soc.*, 2009, **131**, 16646–16647.
19 H. Fang, H. Cong, M. Suzuki, L. Bao, B. Yu, Y. Xie, N. Mizorogi, M. M. Olmstead, A. L. Balch, S. Nagase, T. Akasaka and X. Lu, *J. Am. Chem. Soc.*, 2014, **136**, 10534–10540.
20 K. Tan and X. Lu, *J. Phys. Chem. A*, 2006, **110**, 1171–1176.
21 W. Xu, T.-S. Wang, J.-Y. Wu, Y.-H. Ma, J.-P. Zheng, H. Li, B. Wang, L. Jiang, C.-Y. Shu and C.-R. Wang, *J. Phys. Chem. C*, 2011, **115**, 402–405.
22 K. Junghans, C. Schlesier, A. Kostanyan, N. A. Samoylova, Q. Deng, M. Rosenkranz, S. Schiemenz, R. Westerström, T. Greber, B. Büchner and A. A. Popov, *Angew. Chem., Int. Ed.*, 2015, **54**, 13411–13415.
23 K. Junghans, K. B. Ghiassi, N. A. Samoylova, Q. Deng, M. Rosenkranz, M. M. Olmstead, A. L. Balch and A. A. Popov, *Chem.–Eur. J.*, 2016, **22**, 13098–13107.
24 A. A. Popov, L. Zhang and L. Dunsch, *ACS Nano*, 2010, **4**, 795–802.
25 Y.-J. Guo, H. Zheng, T. Yang, S. Nagase and X. Zhao, *Inorg. Chem.*, 2015, **54**, 8066–8076.
26 S. T. Liddle, *Molecular metal-metal bonds*, Wiley-VCH Verlag GmbH & Co. KGaA, 2015.
27 C.-S. Cao, Y. Shi, H. Xu and B. Zhao, *Coord. Chem. Rev.*, 2018, **365**, 122–144.
28 M. V. Butovskii and R. Kempe, *New J. Chem.*, 2015, **39**, 7544–7558.
29 S. Hu, P. Zhao, W. Shen, P. Yu, W. Huang, M. Ehara, Y. Xie, T. Akasaka and X. Lu, *Nanoscale*, 2019, **11**, 13415–13422.
30 S. Yang, C. Chen, A. Popov, W. Zhang, F. Liu and L. Dunsch, *Chem. Commun.*, 2009, 6391–6393.
31 C. Chen, F. Liu, S. Li, N. Wang, A. A. Popov, M. Jiao, T. Wei, Q. Li, L. Dunsch and S. Yang, *Inorg. Chem.*, 2012, **51**, 3039–3045.
32 F. Liu, T. Wei, S. Wang, J. Guan, X. Lu and S. Yang, *Fullerenes, Nanotubes, Carbon Nanostruct.*, 2014, **22**, 215–226.
33 Y.-Y. Xu, H.-R. Tian, S.-H. Li, Z.-C. Chen, Y.-R. Yao, S.-S. Wang, X. Zhang, Z.-Z. Zhu, S.-L. Deng, Q. Y. Zhang, S. F. Yang, S.-Y. Xie, R.-B. Huang and L.-S. Zheng, *Nat. Commun.*, 2019, **10**, 485.
34 Y. Iiduka, T. Wakahara, T. Nakahodo, T. Tsuchiya, A. Sakuraba, Y. Maeda, T. Akasaka, K. Yoza, E. Horn, T. Kato, M. T. H. Liu, N. Mizorogi, K. Kobayashi and S. Nagase, *J. Am. Chem. Soc.*, 2005, **127**, 12500–12501.
35 T. Wang, J. Wu, W. Xu, J. Xiang, X. Lu, B. Li, L. Jiang, C. Shu and C. Wang, *Angew. Chem., Int. Ed.*, 2010, **49**, 1786–1789.
36 B. Wu, T. Wang, Y. Feng, Z. Zhang, L. Jiang and C. Wang, *Nat. Commun.*, 2015, **6**, 6468.
37 E. Nishibori, I. Terauchi, M. Sakata, M. Takata, Y. Ito, T. Sugai and H. Shinohara, *J. Phys. Chem. B*, 2006, **110**, 19215–19219.
38 S. Taubert, M. Straka, T. O. Pennanen, D. Sundholm and J. Vaara, *Phys. Chem. Chem. Phys.*, 2008, **10**, 7158–7168.
39 R. Shannon, *Acta Crystallogr., Sect. A: Cryst. Phys., Diffr., Theor. Gen. Crystallogr.*, 1976, **32**, 751–767.
40 S. F. Yang, S. I. Troyanov, A. A. Popov, M. Krause and L. Dunsch, *J. Am. Chem. Soc.*, 2006, **128**, 16733–16739.
41 D. N. Laikov and Y. A. Ustynuk, *Russ. Chem. Bull.*, 2005, **54**, 820–826.
42 F. Neese, F. Wennmohs, U. Becker and C. Riplinger, *J. Chem. Phys.*, 2020, **152**, 224108.
43 J. P. Perdew, K. Burke and M. Ernzerhof, *Phys. Rev. Lett.*, 1996, **77**, 3865–3868.
44 F. Weigend and R. Ahlrichs, *Phys. Chem. Chem. Phys.*, 2005, **7**, 3297.
45 M. Dolg, H. Stoll, A. Savin and H. Preuss, *Theor. Chim. Acta*, 1989, **75**, 173–194.
46 J. Yang and M. Dolg, *Theor. Chem. Acc.*, 2005, **113**, 212.
47 T. Zuo, L. Xu, C. M. Beavers, M. M. Olmstead, W. Fu, T. D. Crawford, A. L. Balch and H. C. Dorn, *J. Am. Chem. Soc.*, 2008, **130**, 12992–12997.

48 L. Bao, M. Chen, C. Pan, T. Yamaguchi, T. Kato, M. M. Olmstead, A. L. Balch, T. Akasaka and X. Lu, *Angew. Chem., Int. Ed.*, 2016, **55**, 4242–4246.

49 F. Liu, G. Velkos, D. S. Krylov, L. Spree, M. Zalibera, R. Ray, N. A. Samoylova, C.-H. Chen, M. Rosenkranz, S. Schiemenz, F. Ziegs, K. Nenkov, A. Kostanyan, T. Greber, A. U. B. Wolter, M. Richter, B. Büchner, S. M. Avdoshenko and A. A. Popov, *Nat. Commun.*, 2019, **10**, 571.

50 F. Liu, L. Spree, D. S. Krylov, G. Velkos, S. M. Avdoshenko and A. A. Popov, *Acc. Chem. Res.*, 2019, **52**, 2981–2993.